Journal of Photochemistry and Photobiology A: Chemistry 228 (2012) 60–67

Contents lists available at SciVerse ScienceDirect

Journal of Photochemistry and Photobiology A: Chemistry

journal homepage: www.elsevier.com/locate/jphotochem

Functionalised, photostable, fluorescent polystyrene nanoparticles of narrow size-distribution

Michal Pellach, Jenny Goldshtein, Ofra Ziv-Polat, Shlomo Margel*

Department of Chemistry, Bar-Ilan Institute of Nanotechnology and Advanced Materials, Bar-Ilan University, Ramat Gan 52900, Israel

ARTICLE INFO

Article history:
Received 12 May 2011
Received in revised form
20 November 2011
Accepted 24 November 2011
Available online 13 December 2011

Keywords:
Fluorescent nanoparticles
Polystyrene nanoparticles
Fluorescein
Emulsion polymerisation

ABSTRACT

Fluorescent nanoparticles continue to be of wide interest, as they have many advantages over single fluorescent molecules for biological imaging and sensing applications, such as increased fluorescence intensity and reduced photobleaching. In the following work, styrene was copolymerised with a newly synthesised, fluorescein-based, vinylic crosslinking monomer, by emulsion polymerisation, to create a series of different sized fluorescent nanoparticles (35–100 nm), each of narrow size-distribution. The particles were found to be highly fluorescent and with lower photobleaching compared to fluorescein isothiocyanate (FITC), offering an attractive alternative. The fluorescence excitation and emission spectra were recorded, being similar to fluorescein, but with interesting variation in the excitation spectra. The particles also have a wide range of potential uses, such as examining particle uptake activity of a macrophage cell line, also demonstrated. The nanoparticles were coated with albumin to provide functionality for potential conjugation to biological targeting agents.

1. Introduction

Fluorescent nanoparticles have attracted much interest in biological imaging, biosensing [1], fluorescent cell sorting and bioanalysis [2] due to their various advantages over single dye molecules, such as increased fluorescence and reduced photobleaching [3,4]. Besides the simple additive effect achieved by confining a large number of fluorescent molecules into a small volume, increasing the fluorescence per particle, dye molecules entrapped within matrix particles have a matrix shielding effect [5] from molecular oxygen, which reduces formation of reactive oxygen species (ROS) hence reducing photobleaching. The matrix also reduces mobility of the dye molecules reducing the chance of collision, thus reducing fluorescence quenching [4], giving overall increased photostability.

Covalently incorporating dye into particles rather than dye-doping, greatly reduces potential problems such as dye aggregation as well as leakage of dye from within the particles [6], and several research groups have applied this technique. Brambilla et al. synthesised rhodamine B cyanoacetate and covalently incorporated the dye within poly(alkyl cyanoacrylate) nanoparticles, shown to be appropriate for *in vitro* imaging of human brain endothelial cells [6]; mesoporous silica nanoparticles with covalently attached FITC have been prepared, and the particles were successfully uptaken into fibroblast cells [7]; fluorescent nanoparticles have been synthesised using a perylene-based fluorescent monomer [1] as well as bifunctional crosslinker [8]; nanoparticles as potential optical imaging contrast agents have been synthesised, and polystyrene microspheres have also been created, using fluorescent monomers such as fluorescein-based or carbocyanine-based monomers or 4-ethoxyl-*N*-allyl-1,8-naphthalimide, covalently incorporated within the polymeric chains [9,10]. If fluorophores are located within energy-transfer distance to each other, this may lead to quenching [9], however, covalently attaching the dyes to other monomers gives more control over distances between fluorescent moieties.

Fluorescein, and fluorescein isothiocyanate (FITC) are widely used for fluorescence, including biological targeting and imaging, due to their wide accessibility, high quantum yield and FDA approval for *in vivo* use of fluorescein [11–13]. However, its use may be limited due to photobleaching [14,15], the kinetics of which has been studied by Song et al. [16], as well as the limited fluorescent signals obtained from single fluorescent molecules in biological labelling. By incorporating fluorescein into nanoparticles, its advantages can be maintained while minimising effects of bleaching, by slightly modifying the fluorescein molecule. One of the reasons for fluorescein being so prone to photobleaching is the vulnerability of the two phenol groups, which are highly susceptible to attack by radical ROS to form phenoxy radicals [17,18], which can lead to destruction of aromaticity. Therefore, by exchanging the hydroxyl groups with an alternative group photobleaching is expected to be reduced.

* Corresponding author. Tel.: +972 3 5318861; fax: +972 3 5351250.
E-mail address: shlomo.margel@mail.biu.ac.il (S. Margel).

1010-6030/$ – see front matter © 2011 Published by Elsevier B.V.
doi:10.1016/j.jphotochem.2011.11.012

A common method for synthesis of polymeric nanoparticles with narrow size-distribution is by radical emulsion polymerisation. The emulsion polymerisation process begins with the minute amount of insoluble monomer found in the continuous aqueous phase, which, as the oligomeric chain grows, becomes even less soluble and migrates into the surfactant micelles where polymerisation continues. Further oligomeric chains enter between the existing polymeric chains, and again, their polymerisation continues until termination [19]. Controlling factors such as total monomer concentrations, crosslinker concentrations and surfactant concentrations result in variation of the average nanoparticle size [20–23].

The nanoparticles in the following work were prepared by copolymerising a new fluorescent vinylic crosslinking monomer, fluorescein-*O*,*O*-bis-methylstyrene (FBMS), with styrene by emulsion polymerisation. The resulting polystyrene-co-fluorescein-*O*,*O*-bis-methylstyrene (PS-FBMS) nanoparticles synthesised are intensely fluorescent, photostable, and have potential to be exploited in many applications. Here we demonstrated their use in examining particle uptake by a macrophage cell line. We also coated the PS-FBMS particles with albumin, which provided amine and carboxylate functional groups suitable for conjugation of a bioactive agent.

2. Materials and methods

2.1. Materials

The following analytical-grade chemicals were purchased from Sigma–Aldrich and used without further purification: fluorescein (95%), *p*-chloromethyl styrene (97%), tetrahydrofuran (THF, 99.9%), $(Bu)_4NOH$ (40% in H_2O), chloroform ($CHCl_3$ 99%), potassium persulphate (99%), sodium dodecyl sulphate (SDS), styrene (99%), FITC, and BSA. Water was purified by passing deionised water through an Elgastat Spectrum reverse osmosis system (Elga, High Wycombe, UK). Fluorescence intensity measurements and absorbance measurements were performed using a microplate reader with excitation wavelength 485 nm and emission wavelength 535 nm (Spectrafluor Plus, Tecan, Männedorf, Germany). An immunoperoxidase assay kit for determination of albumin in human sera (HSA) (Immunology Consultants Laboratory, Inc.) was used for qualitative determination of BSA. The cell line RAW264 was obtained from ATCC (VA, USA). DMEM, FCS, L-glutamine, penicillin and streptomycin were purchased from Biological Industries, Beit Haemek, Israel.

2.2. Synthesis of FBMS

Synthesis was carried out according to a similar procedure described in the literature [24]. Briefly, fluorescein (0.33 g, 1 mmol) was dissolved in THF (7 mL). A 40% aqueous solution of $(Bu)_4NOH$ was added to the solution and the reaction mixture was stirred at room temperature for 2 h, after which the reaction solvent was evaporated under vacuum. The dry product was dissolved in $CHCl_3$ (5 mL) and the reaction mixture was cooled to 5 °C. *p*-Chloromethylstyrene (0.25 mL, 2 mmol) was added dropwise at temperatures below 5 °C, and the mixture was maintained below 5 °C for 1 h, and then at room temperature for 18 h. Distilled water (10 mL) was added and the product solution was extracted. The product was precipitated from the $CHCl_3$ solution then purified by silica gel chromatography, and its structure was confirmed by NMR (^1H, ^{13}C and 2D, Bruker Avance III–700), low resolution ESI positive mass spectroscopy (QTOF micro, "waters", UK), MALDI High Resolution Mass spectroscopy (using DHB matrix) with external standard of (PEG/OMe)750, Reflection mode, YAG Laser (AutoFlex III Tof/Tof Bruker, Germany) and elemental analysis (EA1110, CE Instruments).

^1H NMR (700 MHz, CD_3OD): δH 8.30 (1H, 19), 7.81 (1H, 17), 7.77 (1H, 18), 7.50 (2H, 34a,b), 7.46 (2H, 33a,b), 7.34 (1H, 16), 7.13 (2H, 26a,b), 7.00 (1H, 8), 6.97 (1H, 11), 6.96 (1H, 1), 6.93 (1H, 10), 6.75 (1H, 28), 6.71 (2H, 25a,b), 6.70 (1H, 36), 6.53 (1H, 2), 6.28 (1H, 4), 5.81 (1H, 29Z), 5.78 (1H, 37Z), 5.28 (1H, 37E), 5.25 (1H, 29E), 5.25 (2H, 31), 4.82 and 4.87 (2H, 23).

^{13}C NMR (175 MHz, CD_3OD): δC 187.20 (3), 166.72 (21), 165.72 (9), 161.17 (5), 155.99 (7), 155.51 (13), 139.30 and 139.28 (27 and 35), 137.75 (36), 137.69 (28), 136.96 (32), 135.06 and 134.92 (15 and 24), 134.08 (17), 132.51 (11), 132.41 (19), 131.71 (20), 131.69 (16), 131.31 (18), 130.75 (1), 129.71 (25a,b), 129.41 (2), 129.02 (33a,b), 127.61 (34a,b), 127.47 (26a,b), 118.26 (14), 116.31 (12), 116.25 (10), 115.04 (37), 114.71 (29), 105.57 (4), 102.59 (8), 71.73 (31), 68.41 (23).

HRMS (M^+, $C_{38}H_{28}O_5$) calculated: 564.63; found: 565.2010. Elemental analysis: calculated C 80.83; H 5.00; O 14.17%; found C 80.86; H 5.01; O 14.11%.

2.3. Synthesis of fluorescent nanoparticles

The fluorescent nanoparticles were synthesised by emulsion polymerisation, with varying ratios of FBMS to styrene, initiator to monomer ratios and total monomer to continuous phase ratios. In a typical experiment, FBMS (10 mg) was dissolved in styrene (1.1 mL) and added to a deaerated solution of potassium persulphate (10 mg) and SDS (50 mg) in water (10 mL). The mixture was polymerised overnight at 73°, to yield nanoparticles of 60 ± 10 nm in diameter. While the mixture appeared uniform, any unpolymerised styrene was removed by disposal of the upper part of the mixture, using a separating funnel. The particles were then passed through a 0.45 μm filter, to remove unpolymerised FBMS, and excess SDS as well as any small amount of monomers remaining in solution were then removed by dialysis. Particle size was varied by manipulation and control of concentrations of both SDS and FBMS.

2.4. Particle characterisation

The hydrodynamic diameter and size distribution of the nanoparticles dispersed in water were determined using a submicron particle analyzer, model N4 Plus, Coulter Electronics Ltd., England. Excitation and emission spectra were measured by a spectrofluorometer (Cary Eclipse).

Thermogravimetric analysis (TGA) and differential scanning calorimetery (DSC) were performed under nitrogen gas, by TGA/DSC STAR^e System (Mettler Toledo, Switzerland).

2.5. Photobleaching experiment

An aqueous solution of FITC (0.01 μM, 100 μL) was prepared, as was a dilute aqueous suspension of PS-FBMS nanoparticles, to give similar fluorescence intensity (FI), at excitation wavelength 460 nm, and emission wavelength of 523 nm (0.02 ± 0.005 mg/mL, 100 μL). The excitation slit was open to 20 nm and the emission slit was open to 5 nm. Each of the samples was illuminated continuously, and FI was measured over a period of twenty minutes by a Cary Eclipse fluorescence spectrophotometer (Agilent Technologies, Inc.).

2.6. Cytotoxicity assay

96-Well plates were seeded with 2×10^5 cells per well of the phagocyte cell line RAW264 in 100 μL DMEM supplemented with

10% foetal calf serum (FCS), 2 mM L-glutamine, 50 units/mL penicillin, and 50 μg/mL streptomycin. After 24 h at 37 °C, nanoparticles in a similar medium to the cells (100 μL) were added, giving total concentrations of 500, 250, 125, 50, 25 and 12.5 μg/mL. After a further 24 h at 37 °C, 3′-[1-(phenylaminocarbonyl)-3,4-tetrazolium]-bis(4-methoxy-6-nitro)benzene-sulphonic acid hydrate (XTT) was added according to kit manufacturer instructions (Biological Industries, Beit Haemek, Israel). Absorbance was read at 450 nm, and the absorbance of corresponding concentrations of PS-FBMS nanoparticles was subtracted from the reading. Cell viability was determined as a percentage of the negative control (untreated cells).

2.7. Uptake of nanoparticles by phagocytes

2.7.1. Cell lines

Cells from the macrophage tumour line RAW264, were grown as adherent cells in tissue culture dishes in a 5% CO_2, 95% air atmosphere at 37 °C, similarly to a previous phagocytosis study [25]. Cultures were transferred biweekly in DMEM supplemented with 10% foetal calf serum (FCS), 2 mM L-glutamine, 50 units/mL penicillin, and 50 μg/mL streptomycin.

2.7.2. Endocytosis assay

100 μL aliquots of the RAW264 cells (1×10^7 cells/mL DMEM-FCS) were dispensed into fluorescence activated cell sorter (FACS) tubes, and 100 μL of PS-FBMS beads [1 mg beads/mL DMEM-FCS] were added to each, and the cultures were incubated at 37 °C for 4–5 h. After incubation, PBS (Ca^{2+}, Mg^{2+} free) was added and the tubes were centrifuged at 1300 rpm for 10 min. The cells were resuspended in PBS (1 mL) and fluorescence was determined by FACS (Gallios™, Beckman Coulter). In addition, 100 μL aliquots of cell preparations, (1×10^5 cells/mL in DMEM-FCS), were dispensed a 24-well plate and incubated at 37 °C. After 24 h, 100 μL of PS-FBMS beads (1 mg beads/mL) were added and the cultures incubated for 4 h at 37 °C. The cells were rinsed with PBS, and then viewed by a digital inverted fluorescent microscope (EVOS, Advanced Microscopy Group).

2.8. Albumin coating

An albumin coating was achieved according to the literature [26], briefly, a mixture of bovine serum albumin (BSA, 10 mg) and PS-FBMS nanoparticles (various sizes, 20 mg) in water (10 mL) was prepared. The mixture was allowed to gradually reach 60°, and was then stirred at 60° overnight, after which the mixture was allowed to cool. Excess albumin was removed by cycles of membrane ultrafiltration, during which the mixture was gradually transferred to PBS.

Qualitative determination of the presence of albumin on the particle surface was performed using an immunoperoxidase assay intended for determination of albumin in human sera (Immunology Consultants Laboratory, Inc.). Briefly, duplicate samples of uncoated as well as BSA coated PS-FBMS nanoparticles (100 μL) were transferred to separate wells containing bound anti-albumin antibody (antiAlb), and allowed to stand at room temperature overnight. The wells were then washed to remove unbound particles, and horseradish peroxidase (HRP) antiAlb conjugate was added. A solution containing 3,3′,5,5′-tetramethylbenzidine and hydrogen peroxide in citric acid buffer at pH 3.3 was added, followed by a 0.3 M sulphuric acid solution, and absorbance was determined at 450 nm.

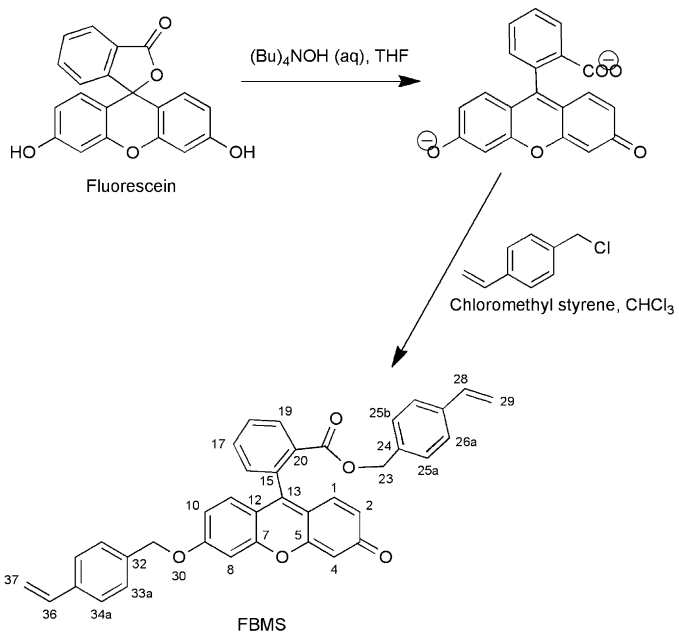

Scheme 1. Synthesis of FBMS.

3. Results and discussion

3.1. Fluorescent crosslinker FBMS

The fluorescent crosslinking monomer was synthesised as described in Section 2, by reaction of fluorescein with *p*-chloromethyl styrene, in basic conditions (Scheme 1). The first step involves deprotonation of fluorescein, opening of the lactone ring and formation of its dianionic form [14,27] The product was a dark orange powder (yield 89%).

Interesting to note is that the hydrogen atoms at C23 are diastereotopic in the NMR spectrum, indicating a biphenyl-like chirality of the molecule. This is due to substitution at the ortho position of the aromatic ring (C20) and hence slow rotation at room temperature about the C13—C15 bond (in the NMR time-scale), due to steric hindrance.

3.2. Synthesis of PS-FBMS nanoparticles

Fluorescent PS-FBMS nanoparticles were synthesised as described in Section 2, by dissolving a small percentage (discussed in the following sections) of FBMS in styrene, followed by emulsion polymerisation. Excess reagents (such as unpolymerised monomer and SDS) were removed by filtration followed by extensive dialysis against water. Variation of concentrations of the fluorescent crosslinker, and concentrations of the surfactant created a series of particles with different fluorescence intensities and of different sizes and size-distributions.

TGA and DSC were performed on the PS-FBMS nanoparticles, and were compared to thermal behaviour of polystyrene. Polystyrene particles were recorded to undergo thermal decomposition at 360–440 °C, whereas those crosslinked with FBMS appeared to decompose at 375–455 °C, showing increased stabilisation against heat, which is probably due to crosslinking of the polystyrene chains. In addition, the glass transition temperature (T_g) of polystyrene is at approximately 110 °C, whereas the lack of a T_g indicates the presence of a crosslinked polymer.

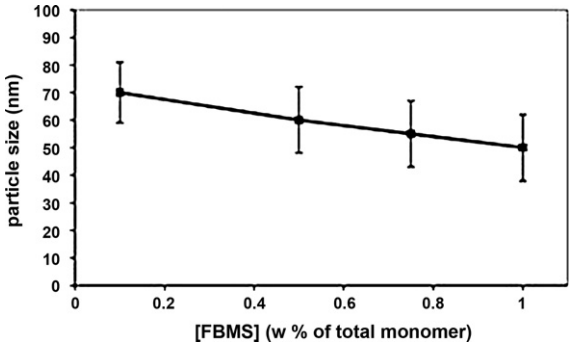

Fig. 1. Variation of average particle size and size distribution by variation of percentage of FBMS, keeping concentrations of initiator, total monomer and volume of continuous phase constant, as described in Section 2.

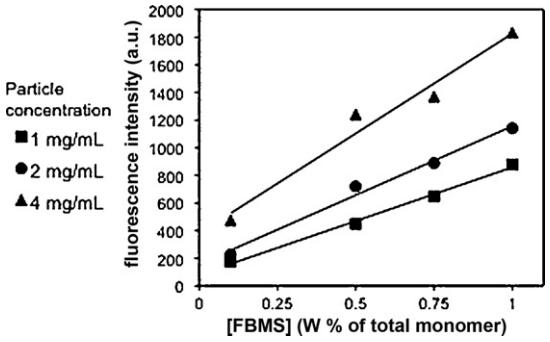

Fig. 2. Effect of percentage of FBMS on FI. A linear increase in FI of the particles was observed with increase in FBMS. Increasing the concentration of particles in water also increased the fluorescent signal, without quenching.

3.3. Effects of variation of FBMS concentration

Variations of crosslinker concentrations while preserving the total monomer concentration may be expected to affect the average particle size. Solutions of 0.1, 0.5, 0.75 and 1.0% (by weight) of FBMS in styrene were prepared at room temperature. At 1.0% (by weight) the solution appears to be saturated, as larger quantities were not successfully dissolved in the styrene. Following polymerisation, the resulting average particle diameters were 70, 60, 55 and 50 nm respectively (Fig. 1), showing only a slight decrease in size, and the size-distribution was also not significantly affected. The trend of a gradual reduction in size is probably due to the decreased ability of the growing nanoparticle to "swell" during the emulsion polymerisation process with an increased percentage of crosslinker.

Fluorescence intensity rarely scales linearly with the number of dye molecules in the particle due to factors such as singlet–singlet annihilation, self-quenching and Stern–Volmer quenching [1]. However, when the fluorescent moiety is kept at low concentrations relative to the non-fluorescent monomer, when integrated into a polymer, FI may be increased with an increase in fluorescent dye, as the non-fluorescent monomer maintains a certain distance between the fluorescent moieties, thus preventing aggregation and fluorescence quenching. The quantum yield of FBMS was found to be 0.67, using fluorescein as a standard with a quantum yield of 0.97 [28]. Despite its lower quantum yield, incorporation of several FBMS molecules would result in significant increase in FI per particle compared to a single fluorescein molecule, if no significant quenching or non-emissive energy transfer takes place.

For nanoparticles prepared using 0.1, 0.5, 0.75 and 1.0% (by weight) of FBMS in styrene, the relative FI was measured for similar particle concentrations (mg/mL). There appeared to be a linear increase in intensity with an increase in concentration of FBMS, with no fluorescence quenching observed (Fig. 2). This can be explained in that the polystyrene chains provide sufficient separation between the fluorescein (FBMS) moieties, so non-emissive energy transfer cannot take place. In experiments that followed, FBMS concentrations used were 1.0% (by weight, 0.2 mmol/mol styrene), in attempt to create the particles with highest FI.

3.4. SDS concentration and particle size

As is well documented, particle size decreases with increasing surfactant concentration [21,29–32]. Besides the tightly packed surfactant molecules affecting growth during particle formation [21], the smaller the particle, the greater the number of SDS molecules required per unit of surface area for particle stabilisation [32]. Variation of SDS concentration was found to be an effective method for obtaining average particle diameters in the range of

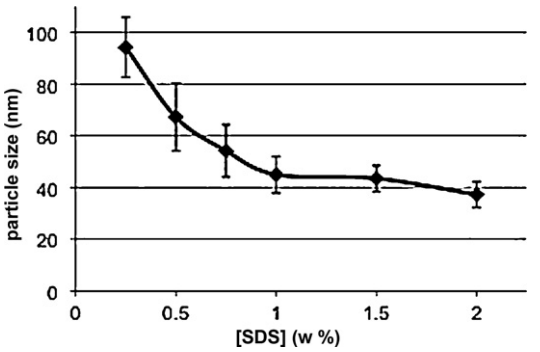

Fig. 3. Effect of SDS concentration on particle size. A non-linear decrease in particle size was observed with increasing concentrations of SDS, while initiator concentration, and volumes of styrene and of aqueous continuous phase are kept constant.

approximately 40–100 nm, while keeping constant initiator and total monomer concentrations. In an experiment using 1% initiator relative to the monomer, and 15 mL of aqueous continuous phase with 0.25, 0.5, 0.75, 1, 1.5 and 2% SDS, particles of average diameter, 94, 67, 54, 45, 44 and 37 nm respectively (Fig. 3). PS-FBMS nanoparticles, at approximate concentrations of 67 mg/mL gave an orange to yellow suspension, depending on particle size. The smaller particles gave a darker translucent suspension, whereas the larger particles gave a lighter opaque suspension (qualitatively illustrated in Fig. 4).

3.5. Photobleaching

The spectrofluorometer measurements of FI for FITC and for the PS-FBMS nanoparticles were plotted against time over a twenty-minute period. While for both FITC and the nanoparticles the photobleaching appeared to be slow, the decrease in FI was significantly slower for the nanoparticles, which over the twenty minutes

Fig. 4. Appearance of aqueous PS-FBMS nanoparticles (67 mg/mL) of increasing size (35 ± 5 nm (left) to 87 ± 12 nm (right)).

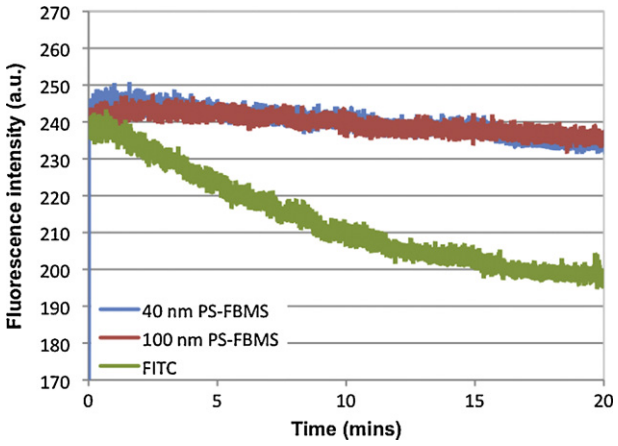

Fig. 5. Photobleaching kinetics of 0.01 μM aqueous FITC (100 μL) compared to 0.2 mg/mL aqueous PS-FBMS nanoparticle suspensions (100 μL).

decreased by approximately five percent and more linear compared to the FITC, which decreased more rapidly by about twenty percent, and the FI graph gradually plateaus (Fig. 5).

It has been shown that there are two major pathways for loss of excited-state fluorescein: reaction between a triplet-state dye molecule with another dye molecule, and reaction between a triplet dye and an oxygen molecule [16]. In the PS-FBMS nanoparticles, the dye–oxygen interaction is greatly reduced due to the polystyrene shielding, and dye–dye interactions are practically eliminated due to the covalent incorporation of the fluorescent moieties and their lack of mobility. Furthermore, The excitation wavelength used was the particles' excitation maximum, rather than that of aqueous FITC (460 rather than 494). On illumination at the FITC excitation maximum one would expect a more rapid decrease in FI, and an even slower loss of fluorescence of the particles.

3.6. Fluorescence spectra

3.6.1. "Solvatochromic" effects

The fluorescence spectra were obtained for fluorescein, the fluorescent crosslinker in solution, as well as incorporated within PS nanoparticles (Fig. 6). Interestingly, when comparing, the spectrum of fluorescein in EtOH is similar to that of FBMS in EtOH, with no significant shifts in the excitation and emission maxima. The optical spectra of fluorescent molecules are often affected by their medium, as changes in polarity of the medium result in changes in the electronic state or dipole moments of the fluorescent moieties, which consequently results in shifts of peak maxima [14,33–35]. Although the FBMS moiety is slightly modified after polymerisation, a shift is demonstrated with the spectrum of FBMS within non-polar PS. Note that once dye is incorporated into polymeric particles, it no longer interacts with the solvent in which the particles are dispersed, and therefore the media in which the particles are dispersed does not affect the fluorescence spectra, that is, solvatochromism is generally not relevant for these polystyrene-based fluorescent particles, unless the solvent is able to penetrate them.

Also worth noting, is that the stokes shift of fluorescein in EtOH, as shown in Fig. 6, is approximately 67 nm, which is advantageous over the usual 22–24 nm observed for aqueous FITC, however, its use is limited partly because of its lack of solubility in aqueous solution. The stokes shift of the PS-FBMS nanoparticles is similar to that of fluorescein in EtOH (approximately 70 nm), allowing excitation as well as detection at the particles' maxima, and thus full exploitation of their fluorescent

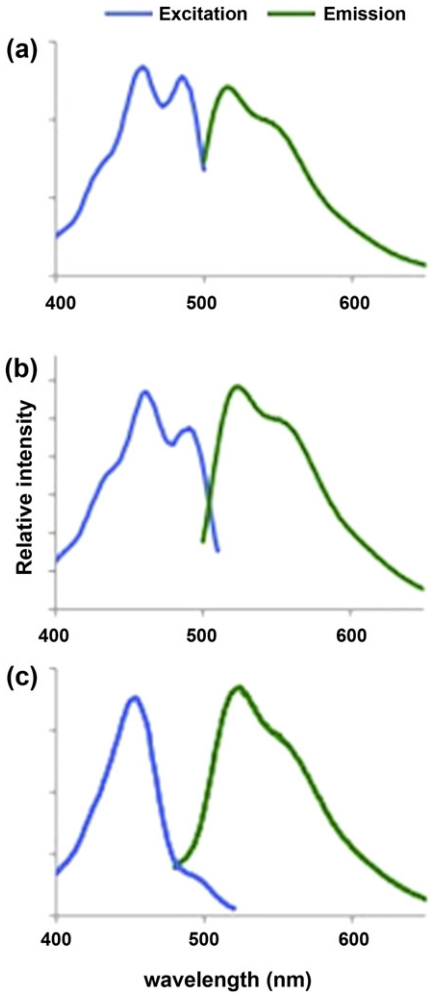

Fig. 6. Optical spectra for (a) fluorescein in EtOH. Excitation λ_{max} = 458(485) nm, emission λ_{max} = 515 nm, (b) FBMS in EtOH. Excitation λ_{max} = 460(488) nm, emission λ_{max} = 521, and (c) an aqueous suspension of PS-FBMS nanoparticles of average diameter 50 nm. Excitation λ_{max} = 452 nm, emission λ_{max} = 521.

properties, while also having dispersibility in an aqueous phase.

3.6.2. Particle size and optical effects

The original precipitated product (see Section 2.2) contained approximately ten percent of the monoalkylated product fluorescein methyl styrene (FMS, molecular weight 449 by MS) monomer (with alkylation presumably at O22, Scheme 1). Following polymerisation using this product mixture, the emission spectrum of the obtained nanoparticles was found to be a shouldered peak (as in the spectra in Fig. 6), and again approximately equivalent for each of the particle sizes. The excitation spectra, however, showed a size-dependence for the PS-FBMS-FMS nanoparticles, with a secondary excitation peak appearing similar in intensity to the primary peak for the 100 nm particles, and then decreasing in intensity as particle size is reduced (Fig. 7). A possible explanation of this phenomenon is that the monoalkylated fluorescent moiety is less protected by polystyrene chains. The larger particles' polystyrene chains are relatively extended, maintaining distance between the fluorescent moieties. As the particle size decreases, there is increased folding of the polymeric chains within the particle, allowing an increasing number of the monosubstituted moieties to reach energy-transfer distances between fluorescent moieties, and to quench each other's fluorescence.

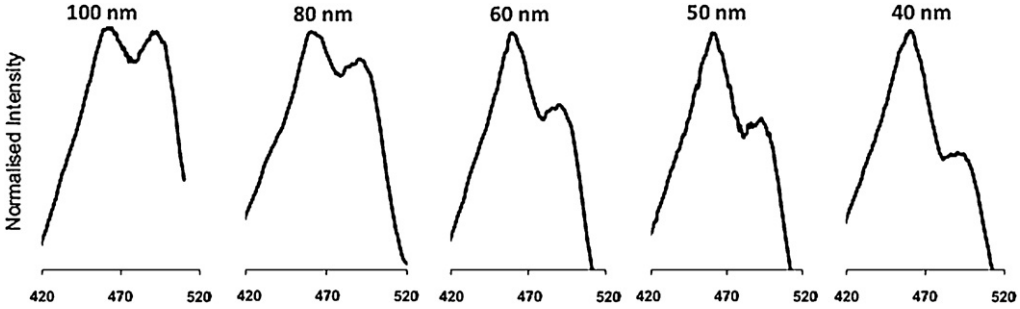

Fig. 7. Normalised excitation spectra of PS-FBMS-FMS nanoparticles. Larger particles have a secondary peak appearing similar in intensity to the primary peak, and the secondary peak decreases in intensity relative to the primary peak, as the particle size decreases.

3.7. Cytotoxicity assay

An XTT assay for determining the effect of PS-FBMS nanoparticles on cell viability was performed, as described in Section 2. After 24 h of exposure of the phagocyte cell line RAW264 to the nanoparticles, no significant toxicity was observed for nanoparticle concentrations of up to 125 μg/mL. Minor toxicity was observed for concentrations of 250 and 500 μg/mL, with approximately 80% and 75% cell viability, respectively (Fig. 8).

3.8. Uptake of nanoparticles by phagocytes

A macrophage cell line (RAW264) was treated with different sized PS-FBMS nanoparticles, as described in Section 2. The macrophage cells were found to gain fluorescence due to the uptaken PS-FBMS nanoparticles (Fig. 9). The larger the particles, the greater the percentage of cells that obtained fluorescence and the greater their FI (Fig. 10a). A kinetic study showing increasing fluorescence over 5 h indicated continued internalisation of nanoparticles (Fig. 10b). With illumination of the cells over several minutes, no loss of fluorescence was observed due to photobleaching.

3.9. Albumin coating

The uncoated particles are stabilised in the aqueous phase due to the negatively charged SDS molecules that remain on the particle surface, in slightly acidic aqueous conditions. For most biological labelling, the particles require a buffered environment, that is, positive and negative ions that affect both the pH of the solution as well as the charge of the particle surface, and hence the ability of SDS molecules to stabilise the particles. Transferring the particles to PBS thus leads to particle destabilisation and aggregation. The albumin coating, with both positive and negative charges at physiological pH, provides a more "buffer friendly" particle surface, and stabilises the particles in aqueous buffer solutions such as PBS. The main function of the proteinaceous coating, though, is to provide functional groups such as amines and carboxyl groups for conjugation of a desired targeting agent.

The albumin coating was verified as described in Section 2. Although the method used was for un-denatured HSA, and the protein in question was denatured BSA, the method was predicted to be effective for qualitative analysis, due to sequential and structural similarities between BSA and HSA [36]. The average absorbance for uncoated particles at 450 nm was 0.095 (a.u.) compared to 0.145 (a.u.) for coated particles. As expected, the use of denatured BSA

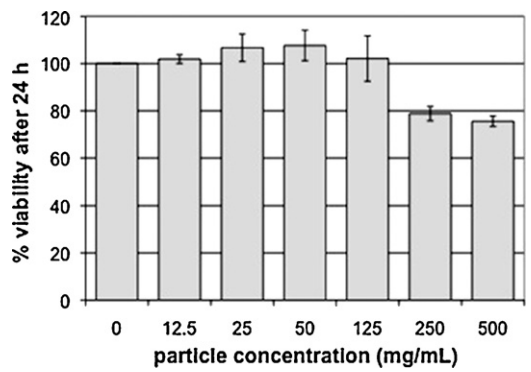

Fig. 8. Viability of cells exposed to PS-FBMS nanoparticles, after 24 h, expressed as a percentage of the negative control.

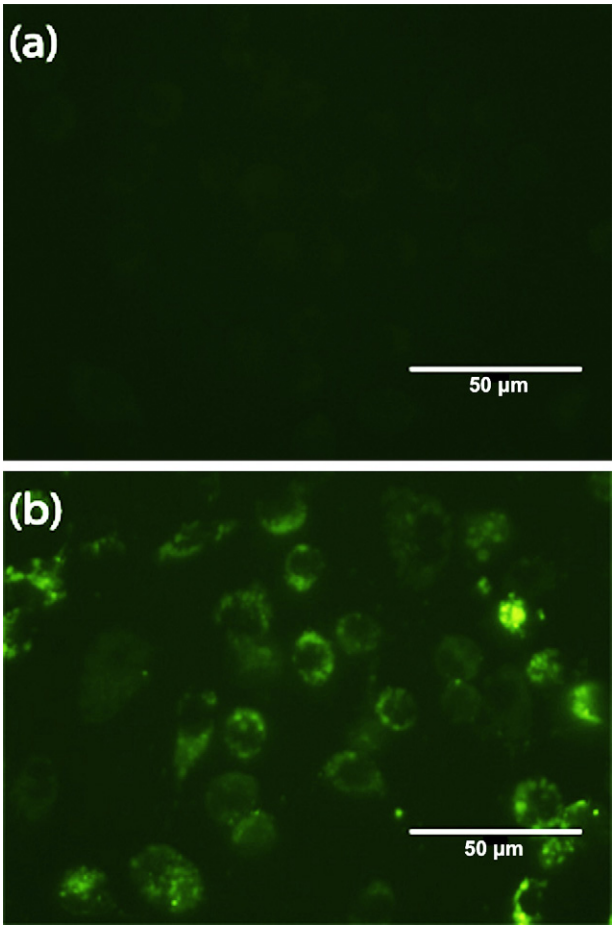

Fig. 9. Fluorescent microscopy of RAW264 macrophages without (a) and containing (b) uptaken 60 ± 12 nm PS-FBMS nanoparticles. The figure shows that the particles have been internalised into the cells and are not merely adsorbed onto the cell surface.

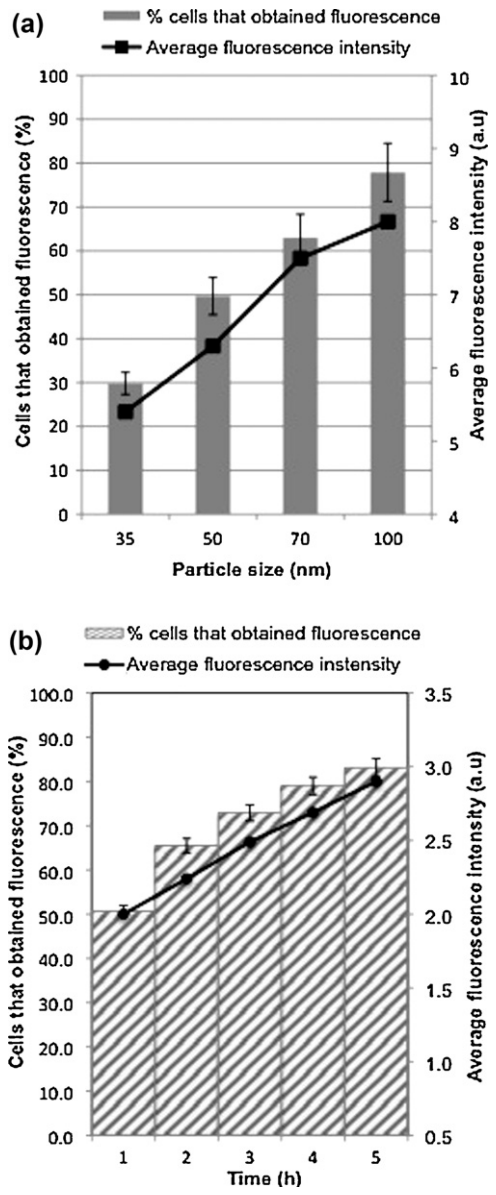

Fig. 10. Phagocytosis of PS-FBMS nanoparticles by RAW264 macrophage cells. Dependence on particle size (a) and kinetic study showing increase in fluorescence over time due to phagocytotic uptake of PS-FBMS 60 ± 12 nm nanoparticles (b).

resulted in a weakened signal compared to what would be expected if detecting natured HSA. However, results were reproducible, and conclusive to our satisfaction, indicating the presence of albumin on the particle surface, and thus functional groups for conjugation to a biological targeting agent, for imaging purposes. The influence of an albumin coating on endocytosis of the particles was unclear, and further investigation of this is required.

4. Conclusions

Fluorescent PS-FBMS fluorescent, crosslinked nanoparticles may be synthesised by emulsion copolymerisation of styrene with a fluorescein-based crosslinking monomer, and their size is easily manipulated. Their biocompatibility together with their non-biodegradability makes them ideal as biological imaging agents, with an increased lifetime in biological settings. Compared to commonly used FITC, the particles' emission wavelength is similar, so methods used for detection are similar, however the particles' excitation maximum is at 452 nm giving a significant increase in Stokes shift. Each particle also has greater fluorescence and greater photostability compared to a single FITC molecule.

Functionalisation of the particles is provided by an albumin coating, which provides both carboxyl and amine groups that may be used for conjugation of a bioactive agent. In the future, the bioactivated fluorescent nanoparticles can then be used in various biomedical applications such as diagnostics, drug targeting, cellular labelling and cell separation [3,37]. Overall, the PS-FBMS nanoparticles are promising fluorescent nanomaterials that are easily synthesised, bright, photostable and size-tuneable with a variety of potential uses.

Acknowledgements

Thanks to Dr. Hugo Gottlieb for his assistance in NMR spectroscopy analysis and structure elucidation. Also thanks to Dr. Igor Grinberg for his assistance in performing cytotoxicity assays.

Appendix A. Supplementary data

Supplementary data associated with this article can be found, in the online version, at doi:10.1016/j.jphotochem.2011.11.012.

References

[1] Z. Tian, A.D. Shaller, A.D.Q. Li, Twisted perylene dyes enable highly fluorescent and photostable nanoparticles, Chemical Communications (2009) 180–182.
[2] J. Yan, M.C. EstÈvez, J.E. Smith, K. Wang, X. He, L. Wang, W. Tan, Dye-doped nanoparticles for bioanalysis, Nano Today 2 (2007) 44–50.
[3] P. Sharma, S. Brown, G. Walter, S. Santra, B. Moudgil, Nanoparticles for bioimaging, Advances in Colloid and Interface Science 123–126 (2006) 471–485.
[4] E. Rampazzo, S. Bonacchi, M. Montalti, L. Prodi, N. Zaccheroni, Self-organizing core-shell nanostructures: spontaneous accumulation of dye in the core of doped silica nanoparticles, Journal of the American Chemical Society 129 (2007) 14251–14256.
[5] E.İ. Altınoğlu, T.J. Russin, J.M. Kaiser, B.M. Barth, P.C. Eklund, M. Kester, J.H. Adair, Near-infrared emitting fluorophore-doped calcium phosphate nanoparticles for in vivo imaging of human breast cancer, ACS Nano 2 (2008) 2075–2084.
[6] D. Brambilla, J. Nicolas, B. Le Droumaguet, K. Andrieux, V. Marsaud, P.-O. Couraud, P. Couvreur, Design of fluorescently tagged poly(alkyl cyanoacrylate) nanoparticles for human brain endothelial cell imaging, Chemical Communications 46 (2010) 2602–2604.
[7] Y. Lin, C. Tsai, H. Huang, C. Kuo, Y. Hung, D. Huang, Y. Chen, C. Mou, Well-ordered mesoporous silica nanoparticles as cell markers, Chemistry of Materials 17 (2005) 4570–4573.
[8] L. Zhu, W. Wu, M. Zhu, J.J. Han, J.K. Hurst, A.D.Q. Li, Reversibly photoswitchable dual-color fluorescent nanoparticles as new tools for live-cell imaging, Journal of the American Chemical Society 129 (2007) 3524–3526.
[9] G. Sun, M.Y. Berezin, J. Fan, H. Lee, J. Ma, K. Zhang, K.L. Wooley, S. Achilefu, Bright fluorescent nanoparticles for developing potential optical imaging contrast agents, Nanoscale 2 (2010) 548–558.
[10] C. Zhao, X. Liu, M. Yang, J. Fang, J. Zhang, F. Liu, The preparation of copolymerized fluorescent microspheres of styrene using detergent-free emulsion polymerization, Dyes and Pigments 82 (2009) 134–141.
[11] G.J. Kapadia, H. Tokuda, R. Sridhar, V. Balasubramanian, J. Takayasu, P. Bu, F. Enjo, M. Takasaki, T. Konoshima, H. Nishino, Cancer chemopreventive activity of synthetic colorants used in foods, pharmaceuticals and cosmetic preparations, Cancer Letters 129 (1998) 87–95.
[12] O.N. Burchak, L. Mugherli, F. Chatelain, M.Y. Balakirev, Fluorescein-based amino acids for solid phase synthesis of fluorogenic protease substrates, Bioorganic and Medicinal Chemistry 14 (2006) 2559–2568.
[13] X. Du, H. Zhang, X. Guo, Y. Deng, H. Wang, 6-Oxy-(acetyl piperazine) fluorescein as a new fluorescent labeling reagent for free fatty acids in serum using high-performance liquid chromatography, Journal of Chromatography 1169 (2007) 77–85.
[14] N. Klonis, A.H.A. Clayton, E.W. Voss, W.H. Sawyer, Spectral properties of fluorescein in solvent–water mixtures: applications as a probe of hydrogen bonding environments in biological systems, Photochemistry and Photobiology 67 (1998) 500–510.
[15] R.S. Davidson, J.E. Pratt, The effects of enzymes on the photobleaching of fluorescein and fluorescein isothiocyanate conjugates, Journal of Photochemistry and Photobiology B: Biology 1 (1988) 361–369.
[16] L. Song, E.J. Hennink, I.T. Young, H.J. Tanke, Photobleaching kinetics of fluorescein in quantitative fluorescence microscopy, Biophysics Journal 68 (1995) 2588–2600.
[17] K.U. Ingold, Inhibition of the autoxidation of organic substances in the liquid phase, Chemical Reviews 61 (1961) 563–589.

[18] G. Scott, Antioxidants, Bulletin of the Chemical Society of Japan 61 (1988) 165–170.
[19] L. Boguslavsky, S. Baruch, S. Margel, Synthesis and characterization of polyacrylonitrile nanoparticles by dispersion/emulsion polymerization process, Journal of Colloid and Interface Science 289 (2005) 71–85.
[20] F. Qian, F. Cui, C. Yin, Preparation, characterization and enzyme inhibition of methylmethacrylate copolymer nanoparticles with different hydrophilic polymeric chains, European Polymer Journal 42 (2006) 1653–1661.
[21] A. Galperin, D. Margel, J. Baniel, G. Dank, H. Biton, S. Margel, Radiopaque iodinated polymeric nanoparticles for X-ray imaging applications, Biomaterials 28 (2007) 4461–4468.
[22] W.-F. Liu, Z.-X. Guo, J. Yu, Preparation of crosslinked composite nanoparticles, Journal of Applied Polymer Science 97 (2005) 1538–1544.
[23] K.A.V. Zubris, O.V. Khullar, A.P. Griset, S. Gibbs-Strauss, J.V. Frangioni, Y.L. Colson, M.W. Grinstaff, Ease of synthesis, controllable sizes, and in vivo large-animal-lymph migration of polymeric nanoparticles, ChemMedChem 5 (2010) 1435–1438.
[24] S. Striegler, M.G. Gichinga, M. Dittel, Macromolecular salen catalyst with largely enhanced catalytic activity, Organic Letters 10 (2007) 241–244.
[25] M. Ito, P. Ralph, M.A.S. Moore, In vitro stimulation of phagocytosis in a macrophage cell line measured by a convenient radiolabeled latex bead assay, Cellular Immunology 46 (1979) 48–56.
[26] O. Ziv-Polat, M. Topaz, T. Brosh, S. Margel, Enhancement of incisional wound healing by thrombin conjugated iron oxide nanoparticles, Biomaterials 31 (2010) 741–747.
[27] M. Krol, M. Wrona, C.S. Page, P.A. Bates, Macroscopic *p*Ka calculations for fluorescein and its derivatives, Journal of Chemical Theory and Computation 2 (2006) 1520–1529.
[28] P. Meallier, S. Guittonneau, C. Emmelin, T. Konstantinova, Photochemistry of fluorescein and eosin derivatives, Dyes and Pigments 40 (1999) 95–98.
[29] H. Ono, E. Jidai, K. Shibayama, Preparation and characterisation of styrene–methyl methacrylate and styrene–methacrylic acid copolymer latices, British Polymer Journal 7 (1975) 109–117.
[30] K. Kato, H. Kondo, A. Morita, K. Esumi, K. Meguro, Synthesis of polystyrene latex with amphoteric surfactant and its characterization, Colloid and Polymer Science 264 (1986) 737–742.
[31] C.U. Kim, J.M. Lee, S.K. Ihm, Emulsion polymerization of tetrafluoroethylene: effects of reaction conditions on particle formation, Journal of Fluorine Chemistry 96 (1999) 11–21.
[32] A.J.P. van Zyl, D.D. Wet-Roos, R.D. Sanderson, B. Klumperman, The role of surfactant in controlling particle size and stability in the miniemulsion polymerization of polymeric nanocapsules, European Polymer Journal 40 (2004) 2717–2725.
[33] P.D. Zoon, A.M. Brouwer, Paradoxical solvent effects on the absorption and emission spectra of amino-substituted perylene monoimides, ChemPhysChem 6 (2005) 1574–1580.
[34] M.A. Rauf, J.P. Graham, S.B. Bukallah, M.A.S. Al-Saedi, Solvatochromic behavior on the absorption and fluorescence spectra of Rose Bengal dye in various solvents, Spectrochimica Acta Part A: Molecular and Biomolecular Spectroscopy 72 (2009) 133–137.
[35] S. Calus, K.S. Danel, T. Uchacz, A.V. Kityk, Optical absorption and fluorescence spectra of novel annulated analogues of azafluoranthene and azulene dyes, Materials Chemistry and Physics 121 (2010) 477–483.
[36] S. Sakata, M.Z. Atassi, Immunochemistry of serum albumin. X. Five major antigenic sites of human serum albumin are extrapolated from bovine albumin and confirmed by synthetic peptides, Molecular Immunology 17 (1980) 139–142.
[37] P. Tallury, A. Malhotra, L.M. Byrne, S. Santra, Nanobioimaging and sensing of infectious diseases, Advanced Drug Delivery Reviews 62 (2010) 424–437.